Supporting Information

In-plane optical anisotropy and nonlinear optical effect in 2D $InTeO_3Cl$

Zemin Zheng[a†], Siyuan Li[a†], Jiuxiang Dai[a], Ang Li[a], Xingxing Zhang[a], Mo Cheng[a], Zhitong Jin[a], Lin Zhou[a]**

[a]School of Chemistry and Chemical Engineering, Frontiers Science Centre for Transformative Molecules, Shanghai Jiao Tong University, Shanghai 200240, China

†These authors contributed equally: Zemin Zheng, Siyuan Li

*Corresponding author e-mail: linzhou@sjtu.edu.cn; jinzhitong@sjtu.edu.cn

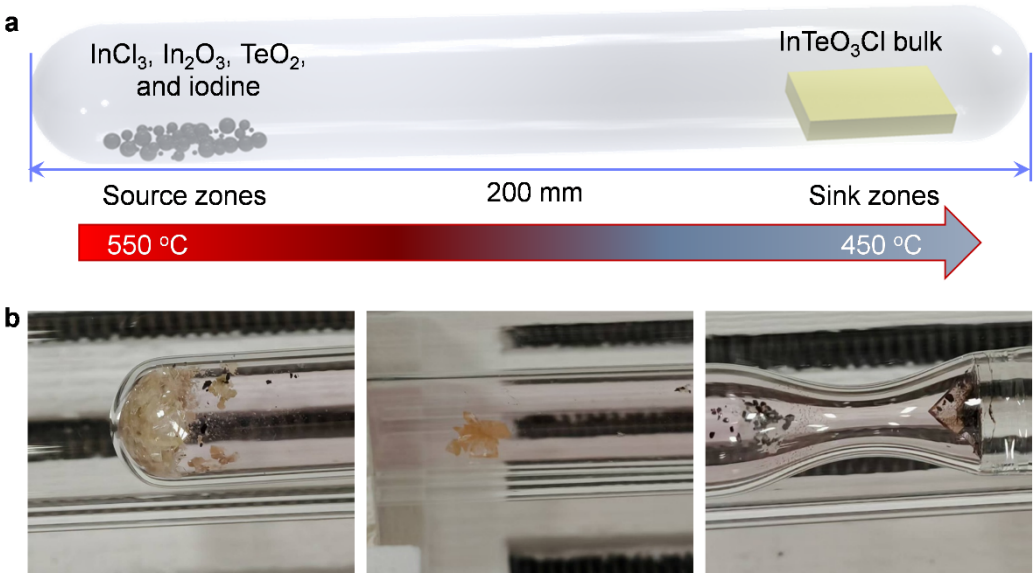

Figure S1. (a) schematically illustrates the chemical vapor transport (CVT) method for the synthesis of $InTeO_3Cl$ crystals and (b) photographs for the different regions of the ampoule after the growth process.

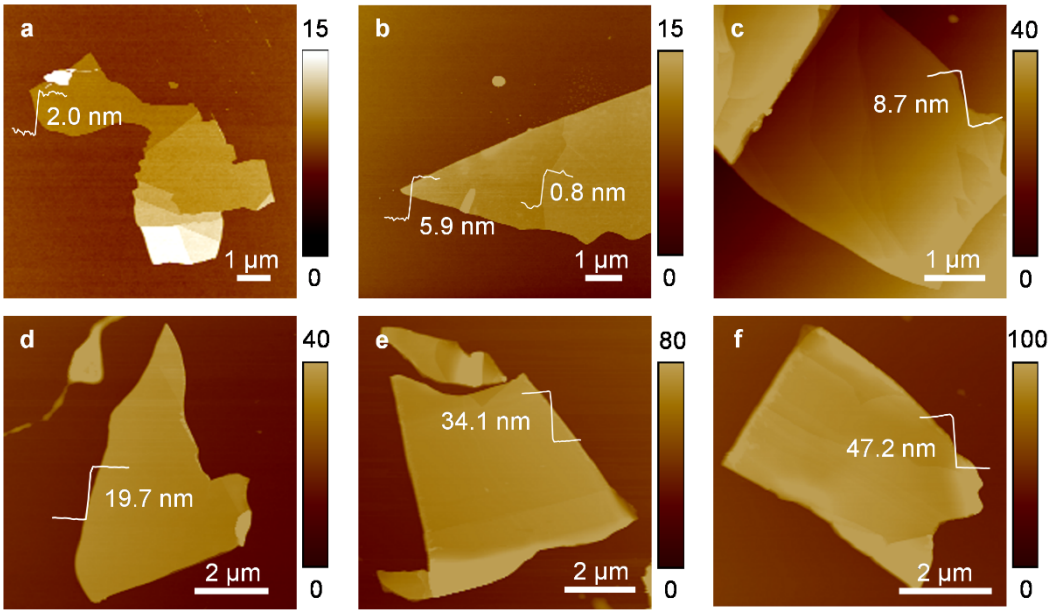

Figure S2. AFM images of exfoliated $InTeO_3Cl$ crystals with varying thicknesses.

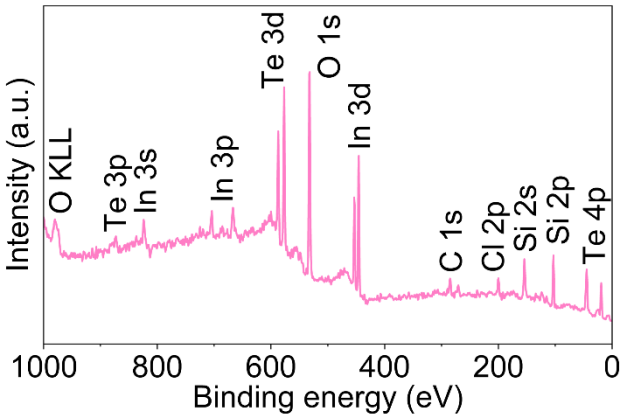

Figure S3. XPS survey spectrum of 2D $InTeO_3Cl$ flakes.

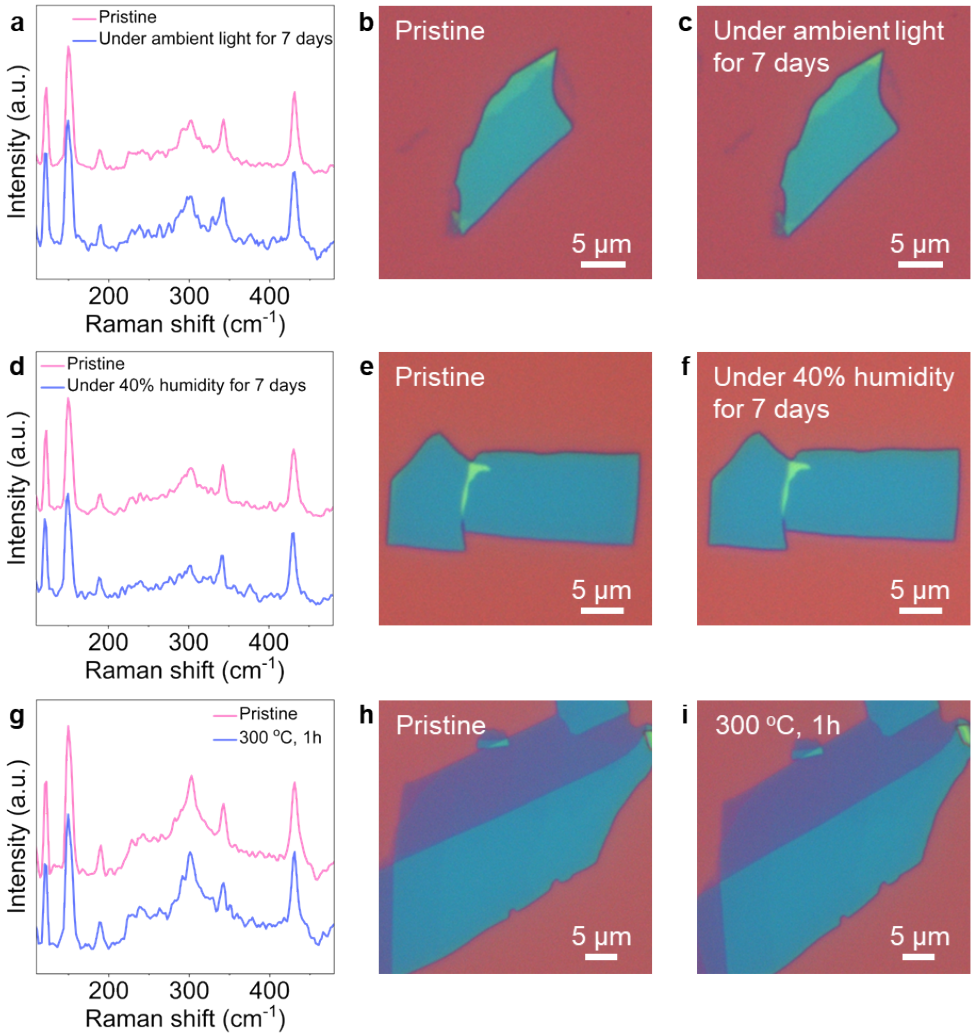

Figure S4. Stability characterizations of $InTeO_3Cl$. Raman spectra (a) and OM images

(b, c) of 2D $InTeO_3Cl$ before and after exposure under ambient light for 7 days. Raman spectra (d) and OM images (e, f) of 2D $InTeO_3Cl$ before and after exposure under about 40% humidity for 7 days. Raman spectra (g) and OM images (h, i) of 2D $InTeO_3Cl$ before and after annealing at 300 ℃ for 1h in Ar.

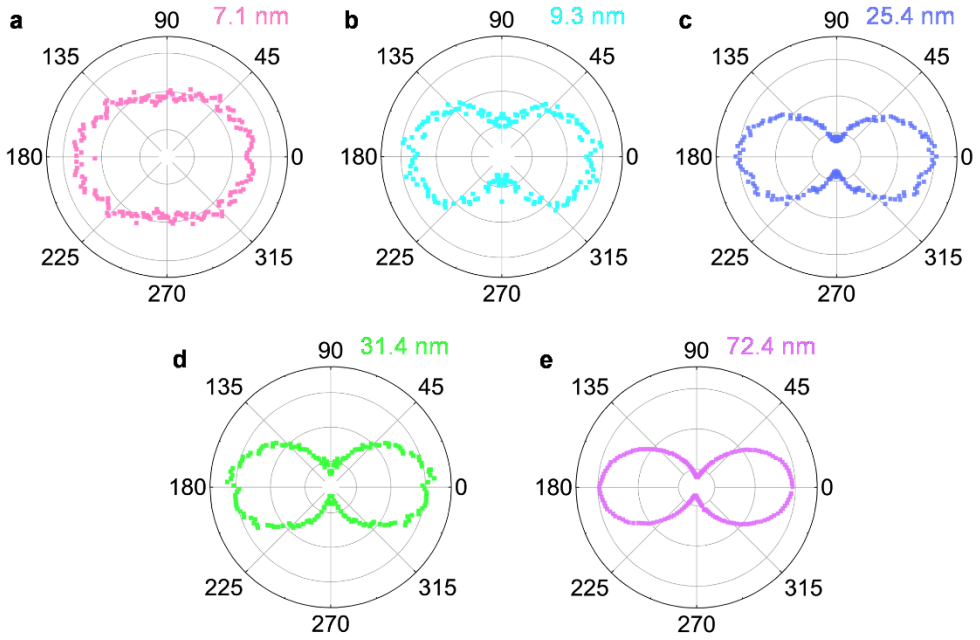

Figure S5. Polar diagram of polarization-dependent SHG intensity of 2D $InTeO_3Cl$ with thicknesses of 7.1 nm (a), 9.3 nm (b), 25.4 nm (c), 31.4 nm (d), and 72.4 nm (e).

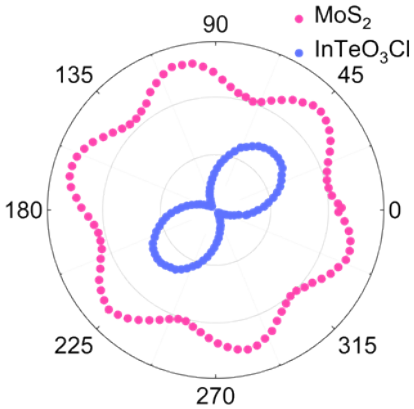

Figure S6. Polar diagram of polarization-dependent SHG intensity of 2D $InTeO_3Cl$ and monolayer MoS_2.

Table S1. The XRD peak positions of prepared $InTeO_3Cl$.

2θ/°	(100)	(200)	(300)
Main peak	11.09	22.19	33.50
Peak 1	10.63	21.26	32.07
Peak 2	10.03	20.03	30.20

Table S2. The lattice distance of (100) plane.

(100)	2θ/°	d/Å	Δd/Å
Main peak	11.09	7.97	
Peak 1	10.63	8.31	0.34
Peak 2	10.03	8.81	0.84